Article:
Matthews, S., Tee, K.L., Rattray, N.J. et al. (5 more authors) (2017) Production of alkenes and novel secondary products by P450 OleT JE using novel H2O2-generating fusion protein systems. FEBS Letters, 591 (5). pp. 737-750. ISSN 0014-5793

https://doi.org/10.1002/1873-3468.12581

Received Date : 08-Nov-2016

Revised Date : 23-Jan-2017

Accepted Date : 26-Jan-2017

Article type : Research Letter

Production of alkenes and novel secondary products by P450 $OleT_{JE}$ using novel H_2O_2-generating fusion protein systems

Sarah Matthews[1], Kang Lan Tee[1], Nicholas J. Rattray[1], Kirsty J. McLean[1], David Leys[1], David A. Parker[2], Richard T. Blankley[3] and Andrew W. Munro[1]*

[1]Manchester Institute of Biotechnology, Centre for Synthetic Biology of Fine and Specialty Chemicals (SYNBIOCHEM), School of Chemistry, The University of Manchester, Manchester M1 7DN, United Kingdom. [2]The Westhollow Technology Center, Houston, Texas 77028-3101, USA. [3]Agilent Technologies UK Ltd., Lakeside, Cheadle Royal Business Park, Stockport, Cheshire SK8 3GR, United Kingdom.

*Author for correspondence: Professor Andrew W. Munro, Phone 0044-161-3065151, Email: Andrew.Munro@Manchester.ac.uk

Abstract

Jeotgalicoccus sp. 8456 $OleT_{JE}$ (CYP152L1) is a fatty acid decarboxylase cytochrome P450 that uses hydrogen peroxide (H_2O_2) to catalyse production of terminal alkenes, which are industrially important chemicals with biofuel applications. We report enzyme fusion systems in which *Streptomyces coelicolor* alditol oxidase (AldO) is linked to $OleT_{JE}$. AldO oxidizes polyols (including glycerol), generating H_2O_2 as a co-product and facilitating its use for efficient $OleT_{JE}$-dependent fatty acid decarboxylation. AldO activity is regulatable by polyol substrate titration, enabling control over H_2O_2 supply to minimise oxidative inactivation of $OleT_{JE}$ and prolong activity for increased alkene production. We also use these fusion systems to generate novel products from secondary turnover of 2-OH and 3-OH myristic acid primary products, expanding the catalytic repertoire of $OleT_{JE}$.

Keywords

$OleT_{JE}$, CYP152L1, cytochrome P450, alkene production, hydrogen peroxide, fusion enzymes

$OleT_{JE}$ peroxygenase P450, alkene production, fusion enzymes

Abbreviations

BSTFA - N,O-*bis*(trimethylsilyl)trifluoroacetamide; DCM – dichloromethane; EDTA - ethylenediaminetetraacetic acid; IPTG - isopropyl 1-thio-ß-D-galactopyranoside; $OleT_{JE}$ – cytochrome P450 $OleT_{JE}$ (CYP125L1) from *Jeotgalicoccus* sp. 8456; P450 – cytochrome P450; TMCS – trimethylchlorosilane; ΔALA – δ-aminolevulinic acid

Introduction

The *Jeotgalicoccus* sp. 8456 $OleT_{JE}$ (CYP152L1) is a member of the cytochrome P450 (P450 or CYP) enzyme superfamily. P450s bind heme *b*, which is proximally coordinated by a cysteine thiolate and typically has a water ligand in the 6^{th} position in the resting state (1). Substrate binding generally displaces the distal water ligand, converting low-spin (LS) ferric heme iron to the high-spin (HS) state (2). The HS heme has a more positive potential, facilitating heme iron reduction by a redox partner, binding of dioxygen to ferrous iron, and subsequent reduction and protonation steps resulting in formation of the ferryl-oxo porphyrin radical species compound I, which is the major substrate oxidizing species in P450s. P450s perform numerous oxidative (and other) reactions, including hydroxylation, demethylation, epoxidation and dehydrogenation of a vast range of substrates (3).

However, not all P450s are redox partner-dependent. Peroxygenase P450s function efficiently using only hydrogen peroxide (H_2O_2) to drive catalysis. Early peroxygenase studies focused on P450-BS_β (CYP152A1) from *Bacillus subtilis* and P450-SP_α (CYP152B1) from *Sphingomonas paucimobilis*. Initial studies suggested these enzymes were fatty acid hydroxylases, using the "peroxide shunt" mechanism to convert substrate-bound, ferric P450 directly to its ferric-hydroperoxo (compound 0) state, which then undergoes rapid protonation and dehydration to form compound I (4,5) (**Figure 1A**). However, Rude et al. subsequently demonstrated that P450-BS_β also produced n-1 terminal alkenes alongside 2-OH and 3-OH fatty acids, suggesting that other CYP152 peroxygenases might also produce alkenes through oxidative decarboxylation of fatty acids (6). The *Jeotgalicoccus* $OleT_{JE}$ P450 was identified as a more efficient alkene producer, catalysing oxidative decarboxylation of fatty acids from ~C10-C20, generating terminal alkenes as major products, with smaller amounts of 2-OH and 3-OH fatty acids (6,7). Terminal alkenes have industrial uses in plastics, lubricants and as feedstocks for other compounds, e.g. alcohols and surfactants (8). Alkenes are also potential fuels, making $OleT_{JE}$ an attractive candidate for production of "drop-in" biofuels (9).

The structure and catalytic mechanism of $OleT_{JE}$ have been characterized (10-12), revealing how the fatty acid carboxylate binds close to the P450 heme (**Figure 1B**), as well as the different mechanisms by which $OleT_{JE}$ produces alkenes and hydroxylated fatty acids. $OleT_{JE}$ was reported to catalyse 97% conversion of 200 μM myristic acid (C14:0) in the presence of 500 μM H_2O_2 (7). However, on an industrial scale excess H_2O_2 may inhibit enzymatic activity (13). This phenomenon was demonstrated

in the *Clostridium actetobutylicum* peroxygenase P450 CLA (CYP152A2) where, despite high peroxygenase activity (200 min^{-1}) with myristic acid, use of 200 µM H_2O_2 caused enzyme inactivation in 2-4 minutes (14). Also, using H_2O_2 in a bacterial cell-based alkene-producing system may not be viable, as H_2O_2 levels of only 2 µM can cause growth inhibition of *E. coli* (15). Girhard et al. described a novel method of driving peroxygenases, using light to excite flavin cofactors with ethylenediaminetetraacetic acid (EDTA) as an electron donor. Electron transfer from reduced flavins then converts dioxygen to H_2O_2. The approach was successful with P450 CLA and P450 BS_β, where near-complete conversion of 200 µM myristic acid was observed using flavin mononucleotide (FMN) (16). This method also worked with $OleT_{JE}$, where 99% of stearic acid (C18:0) substrate was oxidised, a much higher conversion rate than achieved by direct H_2O_2 addition either at the start of the process, or stepwise during the reaction (13). However, this light driven approach produced low conversion levels for the shorter chain substrates lauric acid (C12:0) and myristic acid (13).

In this manuscript, we present novel alkene-producing systems in which the H_2O_2-forming alditol oxidase (AldO) from *Streptomyces coelicolor* is fused to $OleT_{JE}$. AldO is a 45.1 kDa flavoprotein containing covalently bound flavin adenine dinucleotide (FAD) (17). AldO catalyses oxidation of the primary alcohol moiety of alditols using molecular oxygen, and forms the aldose product and H_2O_2. AldO oxidizes several polyol substrates, including glycerol, sorbitol and diols such as 1,2-propanediol and 1,2-hexanediol (18). Our rationale for creating the $OleT_{JE}$-AldO fusion is that the H_2O_2 coproduct from AldO should drive fatty acid decarboxylation by $OleT_{JE}$ and that the system could be regulated through measured alditol substrate additions to maintain H_2O_2 concentrations compatible with efficient substrate conversion, while minimising heme destruction by excess H_2O_2. We present catalytic data showing the efficiency of the reactions, as well as using $OleT_{JE}$ and AldO fusion systems to identify novel products of $OleT_{JE}$-dependent fatty acid oxidation.

Materials and Methods

Gene Cloning

The $OleT_{JE}$ (*CYP152L1*) gene from *Jeotgalicoccus* sp 8456 was codon optimised for expression in *E. coli*, synthesised (Genscript, Cherwell UK) and cloned into pET15b at NdeI/BamHI sites. The construct contains an N-terminal polyhistidine tag and a TEV cleavage site 5' to the NdeI cleavage site. The alditol oxidase (AldO) gene from *Streptomyces coelicolor* A3(2) with an N-terminal polyhistidine tag and TEV cleavage site was codon optimised for *E. coli* expression and synthesised (Genscript), prior to cloning into pET24b at NdeI/BamHI sites.

Cloning of the $OleT_{JE}$-HRV3C-AldO fusion protein gene construct (linker sequence: GSGLEVLFQGPGSGGGGS with cleavage site underlined) was performed by amplification of $OleT_{JE}$/AldO genes from pET15b/pET24b plasmids using primers $OleT_{JE}$-For: GTATTTCCAAGGCCATATG, $OleT_{JE}$-Rev: CCCCTGGAACAGAACTTCCAGACCAGAACCGGTGCGGTC CACAAC, AldO-For: GAAGTTCTGTTCCAGGGGCCCGGATCTGGCGGCGGC, and AldO-Rev: ATTGCGGATCCTTATCAGCCGGCCAG using Phusion High Fidelity DNA polymerase (NEB, Hitchin UK). The 5'-$OleT_{JE}$ and AldO-3' genes were then joined with an HRV3C cleavage site by PCR using primers

GTATTTCCAAGGCCATATG and ATTGCGGATCCTTATCAGCCGGCCAG, respectively. The $OleT_{JE}$-HRV3C-AldO gene was then cloned into the pET15b-TEV plasmid at NdeI/BamHI sites (**Figure 2**).

The $OleT_{JE}$-αhelix-AldO construct was produced using a NEB HiFi DNA assembly Kit (NEB) according to manufacturer's instructions. DNA encoding the $A(EAAAK)_4LEA(EAAAK)_4A$ α-helix was synthesised (Eurofins, Manchester UK). The pET15b $OleT_{JE}$-HRV3C-AldO plasmid was used as a template, and primers ATGTCGGATATTACCGTTACG and GGTGCGGTCCACAACTTC were used to amplify the backbone. The α-helix insert was amplified with backbone overhangs of 15 bp using primers GTTGTGGACCGCACCGCTGAGGCTGCCGCTAAG and ACGGTAATATCCGACATCGCTTTTGCTGCTGCTTC (**Figure 2**).

Gene expression and protein purification

The pET15b-$OleT_{JE}$, pET15b-$OleT_{JE}$-HRV3C-AldO and pET15b-$OleT_{JE}$-αhelix-AldO plasmids were transformed into *E. coli* C41 (DE3) and grown in 500 ml 2xYT cultures. Cultures were shaken at 200 rpm at 37°C until an OD_{600} of 0.5. 500 μM δ-aminolevulinic acid (ΔALA) was added and gene expression induced with 100 μM isopropyl 1-thio-ß-D-galactopyranoside (IPTG). Temperature was decreased to 25°C for pET15b-$OleT_{JE}$ transformed cells, and to 20°C for cells transformed with pET15b-$OleT_{JE}$-HRV3C-AldO and pET15b-OleT-αhelix-AldO constructs. Cells were grown for a further 20 hours before harvesting by centrifugation at 6000 rpm at 4°C in a JLA-8.1 rotor using an Avanti J-26 XP centrifuge. Cell pellets were washed with ice-cold 100 mM KPi buffer (pH 8), centrifuged again and stored at -80°C until required for purification.

Purification of $OleT_{JE}$, $OleT_{JE}$-HRV3C-AldO, $OleT_{JE}$-αhelix-AldO and P450 BM3 heme domain

$OleT_{JE}$ expressing cells were resuspended in 100 mM KPi, 1 M NaCl, 10% glycerol (pH 8) (buffer A). $OleT_{JE}$-HRV3C-AldO and $OleT_{JE}$-αhelix-AldO expressing cells were resuspended in 100 mM KPi, 750 mM NaCl (pH 8) (buffer B). To each cell suspension, SigmaFAST Protease Inhibitor Cocktail Tablets (EDTA-Free), 100 μg/ml DNase I and lysozyme were added (Sigma-Aldrich, Poole UK). Cell suspensions were sonicated for 40 minutes at 10 s on, 50 s off, at 40% amplitude using a Bandelin Sonopuls sonicator. The cell homogenate was then centrifuged at 20,000 rpm for 90 minutes at 4°C using a JA-25.5 rotor.

For $OleT_{JE}$, 5 mM imidazole and nickel-iminodiacetic acid (Ni-IDA) chromatographic medium (Generon, Maidenhead UK) (10 ml/100 g cell pellet) was added to the supernatant and stirred overnight at 4°C. The resin was packed into a column, washed with 20 column volumes (CV) of 50 mM imidazole in buffer C (100 mM KPi, 750 mM NaCl, 10% glycerol [pH 8]) and the flow-through collected. After washing with 2 CV of 150 mM imidazole in buffer C, $OleT_{JE}$ protein was eluted in 175 mM imidazole in buffer C and extensively dialysed into buffer C to remove imidazole and fatty acids retained from *E. coli*. $OleT_{JE}$ was concentrated using a Vivaspin (30,000 MWCO, GE Healthcare, Little Chalfont UK) and transferred into 100 mM KPi, 750 mM NaCl, 20% glycerol (pH 8) (buffer D) using a PD10 Desalting Column (GE Healthcare). The protein was then flash frozen in liquid nitrogen and stored at -80°C.

For $OleT_{JE}$-HRV3C-AldO and $OleT_{JE}$-αhelix-AldO, 5 mM imidazole and Ni-IDA (5 ml/100 g) was added to cell supernatants and samples stirred at 4°C for 2 hours. The resin was washed using 20 CV of 50 mM imidazole in buffer B and the flow-through retained. Proteins were eluted with 250 mM imidazole in buffer B, and incubated overnight at 4°C with ~500 U of a S219V TEV protease variant (expressed using plasmid pRK793, Addgene plasmid no 8827) (19). The protein was exchanged into buffer B using a desalting column, and added to a bed of Ni-IDA resin. His-tag cleaved protein was eluted with 20 mM imidazole in buffer B, concentrated using a Vivaspin (30,000 MWCO) and exchanged into buffer B using a PD10 desalting column. Aliquots were frozen in liquid nitrogen and stored at -80°C.

The *Bacillus megaterium* P450 BM3 heme domain (BM3) and *Mycobacterium tuberculosis* CYP51B1 and CYP121A1 P450s were expressed and purified as described previously (20-22).

Hydrogen peroxide tolerance of P450 enzymes

UV-visible spectroscopy was done on a Cary 60 UV-visible spectrophotometer (Agilent, Cheadle UK). Oxidative modification of $OleT_{JE}$ and other P450 hemes was measured at H_2O_2 concentrations of 25, 50, 75, 125, 250, 500, 1000 and 2000 μM in buffer C. Stock H_2O_2 concentrations were prepared at 500x final concentration. After H_2O_2 addition, P450 spectra were recorded every 1.5 minutes for 1 hour at 10°C. Soret peak intensity (418 nm for $OleT_{JE}$ and CYP51B1, 419 nm for BM3, and 417 nm for CYP121A1) was plotted against time. In each case, data were fitted accurately using a single exponential decay function.

***In vitro* substrate turnover reactions with fusion proteins**

Reactions were done in buffer B. To cleave $OleT_{JE}$-HRV3C-AldO, HRV3C (Novagen, Feltham UK) was added at 1 U/100 μg $OleT_{JE}$-HRV3C-AldO, and incubated for 1 hour at 4°C. Proteins were exchanged into buffer B using a PD10 desalting column before starting reactions.

For reactions with $OleT_{JE}$-HRV3C-AldO and $OleT_{JE}$-αhelix-AldO, 0.5 ml reactions contained 5 μM enzyme, 500 μM myristic acid and varying concentrations of different AldO substrates. Initial studies tested glycerol (3%, 1%, 0.1% and 0.01%), xylitol (2 mM and 10 mM) and sorbitol (2 mM and 10 mM). Reactions were incubated for 20 minutes. Time dependence studies were also done using 1% glycerol at time points of 0.5, 1, 2, 5, 10, 20 and 30 minutes. Additional reactions were done with 0.1% and 0.01% glycerol with incubations for 20 minutes. Time point experiments and reactions with 0.1% and 0.01% glycerol were done in duplicate with incubation at 27°C and shaking at 700 rpm, using 5 μM enzyme and 500 μM myristic acid in a 0.5 ml volume.

Reactions were stopped with 20 μl of 37% HCl. Internal standards 1-pentadecene, palmitic acid (C16:0), 2-OH palmitic acid and 3-OH palmitic acid were added, and reactions were extracted with an equal volume of dichloromethane (DCM). The DCM layer was removed and dried with anhydrous $MgSO_4$. DCM extract was mixed with an equal volume of N,O-*bis*(trimethylsilyl)trifluoroacetamide (BSTFA) containing 1% trimethylchlorosilane (TMCS) and incubated at 60°C for 45 minutes to derivatise fatty acids.

In vitro $OleT_{JE}$ enzymatic reactions with products

To investigate $OleT_{JE}$'s ability to further oxidize initial reaction products, 200 μM 1-tridecene, 200 μM α-OH myristic acid or 200 μM β-OH-myristic acid was incubated with either (i) 1 μM $OleT_{JE}$/500 μM H_2O_2 or (ii) 5 μM $OleT_{JE}$-HRV3C-AldO/1% glycerol. Reaction mixtures were incubated for 30 minutes at 27°C before acidification with 20 μl 37% HCl, and extraction, drying and derivatisation as described previously.

GC/Q-TOF

After derivatisation, 1 μl of sample was injected onto an Agilent 7200 GC/QTOF with 7890B GC, installed with a VF-5ms 30 m x 250 mm x 0.25 mm column. The front inlet was set at 250°C, and a split ratio of 25:1 was used. Column flow was set at 1.2 ml/min, and the oven was held at 100°C for 1 minute before being ramped at 25°C/min until 200°C. Ramping was decreased to 15 ml/min until 325°C, and held for 2 minutes. Electronic ionization was used, and m/z ratios of 40-500 were recorded at 5 Hz and at 230°C. Quantitation of tridecene, myristic acid, α-OH myristic acid and β-OH myristic acid was performed using external standard calibration curves and structural analogue internal standards.

Fusion protein kinetics

To determine reaction kinetics for (i) $OleT_{JE}$-αhelix-AldO and (ii) intact and cleaved forms of $OleT_{JE}$-HRV3C-AldO, decreases in myristic acid substrate concentration were plotted against reaction time. Data were fitted using a single exponential function.

Results

Hydrogen peroxide tolerance

The peroxygenase $OleT_{JE}$ uses H_2O_2 to drive fatty acid decarboxylation. However, excess H_2O_2 oxidatively damages heme and protein. To investigate this phenomenon, H_2O_2 was added to $OleT_{JE}$ at various concentrations from 25-12000 μM, and decreases in Soret peak intensity were monitored. To compare effects of H_2O_2 on $OleT_{JE}$ with other P450s, the experiment was repeated with the fatty acid hydroxylase P450 BM3 heme domain (BM3), and the *M. tuberculosis* P450s CYP51B1 (sterol demethylase) and CYP121A1 (cyclodipeptide oxidase) (20-22). Heme modification was measured at intervals up to one hour, and at 10°C to minimise temperature-related effects on protein stability (**Table 1**). **Figure 3** shows time-dependent changes in UV-visible spectra for $OleT_{JE}$ and the other P450s, demonstrating Soret band absorbance decreases indicative of heme modification. Decreases in P450 Soret peak intensity were plotted against time, and rate constants (*k*) were derived for heme oxidation processes. For $OleT_{JE}$, BM3, CYP51B1 and CYP121A1, data were fitted using a single exponential function. The heme oxidation rate constant (*k*) is consistently lower for $OleT_{JE}$ compared to the other P450s. Differences in H_2O_2 tolerance are most apparent at higher H_2O_2 concentrations

(e.g. k = 8.51 min^{-1} for $OleT_{JE}$ compared to 43.25 min^{-1} for BM3). Moreover, heme oxidation progresses much further for the other P450s than for $OleT_{JE}$ over the same time frame. These data demonstrate that $OleT_{JE}$ has a greater H_2O_2 tolerance than the other bacterial P450 monooxygenases, consistent with its function as a peroxygenase. Some $OleT_{JE}$ heme depletion clearly occurs at 1 mM H_2O_2, and peroxide concentrations in this range are typically used in peroxygenase turnover experiments with fatty acids (10,23). However, more efficient fatty acid oxidation (with less heme destruction) could be achieved in a catalytic system where H_2O_2 is produced (and enzymatically consumed) continuously at a level that is non-destructive to $OleT_{JE}$ heme.

Construction of $OleT_{JE}$-HRV3C-AldO and $OleT_{JE}$-αhelix-AldO fusion proteins

Two fusion proteins ($OleT_{JE}$-HRV3C-AldO and $OleT_{JE}$-αhelix-AldO) were constructed by linking $OleT_{JE}$ to *S. coelicolor* AldO. In these systems, AldO produces H_2O_2 from oxidation of substrates including glycerol, sorbitol and xylitol. H_2O_2 then drives fatty acid decarboxylation by $OleT_{JE}$. The $OleT_{JE}$-HRV3C-AldO fusion contains a short peptide linker incorporating a HRV3C cleavage site. The protease cleavage site enables production of stoichiometric amounts of free $OleT_{JE}$ and AldO, allowing for comparative analysis of the activity of the separated enzymes. The $OleT_{JE}$-HRV3C-AldO protein was produced at ~2.5 mg/L culture. Fusing human growth hormone (hGH) and transferrin (Tf) with a rigid helical linker was shown to be more successful for protein production by comparison to hGH/Tf fusions without a helical linker (24,25). We adopted a similar strategy to produce the $OleT_{JE}$-αhelix-AldO fusion enzyme, which was also purified at ~2.5 mg/L. **Figure 4** shows SDS-PAGE gels of both constructs following purification by Ni-IDA chromatography, TEV cleavage of the polyhistidine tag, and separation of the untagged fusion protein by reverse Ni-IDA chromatography. **Figure 4A** also shows $OleT_{JE}$-HRV3C-AldO following inter-domain cleavage using HRV3C protease.

Driving fatty acid decarboxylation with different AldO substrates

Reactions were set up with 5 μM $OleT_{JE}$-HRV3C-AldO, 0.5 mM myristic acid and different AldO substrates (glycerol, sorbitol and xylitol). An additional reaction was set up with 500 μM H_2O_2 and 5 μM $OleT_{JE}$-HRV3C-AldO. A control reaction without substrate was also set up, including 40 units of catalase to remove any H_2O_2. **Table 2** shows that all AldO substrates gave high levels of turnover, facilitating myristic acid oxidation levels of 91-95%, compared to 87% in the case where H_2O_2 was added directly to substrate-bound $OleT_{JE}$. Glycerol gave marginally the highest levels of substrate oxidation, and was used as the AldO substrate in further experiments.

Time-dependent oxidation of fatty acids using fusion proteins

Reactions were set up with 1% glycerol, 0.5 mM myristic acid, and 5 μM of (i) intact $OleT_{JE}$-HRV3C-AldO, (ii) cleaved $OleT_{JE}$-HRV3C-AldO or (iii) $OleT_{JE}$-αhelix-AldO. Myristic acid concentration was plotted against time, and rate constants (k) determined for fatty acid conversion. The highest rate was obtained for $OleT_{JE}$-αhelix-AldO (0.48 ± 0.02 min^{-1}). $OleT_{JE}$-HRV3C-AldO and the HRV3C-cleaved

forms showed conversion rates of 0.38 ± 0.05 min^{-1} and 0.15 ± 0.01 min^{-1}, respectively, indicating that the fused enzymes have higher activity than their separate entities at the same concentration. **Figure 5** shows GC-MS analysis of myristic acid products formed by the $OleT_{JE}$-αhelix-AldO fusion enzyme.

Product formation over time was also monitored for the conditions (i)-(iii). In all cases, tridecene was the major product after 20 minutes (**Table 3**). However, for both intact and cleaved $OleT_{JE}$-HRV3C-AldO, 3-OH myristic acid is initially produced at high levels, and is the major product at 1 minute. Levels of 2-OH and 3-OH myristic acid decreased after 2 minutes in all three conditions. We hypothesised that, with continued production of H_2O_2 by AldO-dependent glycerol oxidation, the hydroxylated fatty acids are further converted into other products. This finding indicates that the $OleT_{JE}$ protein constructs used remain active throughout the assays and can bind and further oxidise the primary reaction products.

Optimising glycerol concentration for $OleT_{JE}$ activity

To establish suitable glycerol concentrations for $OleT_{JE}$-AldO fusion proteins, reactions were also performed with 0.1 and 0.01% glycerol, and stopped after 20 minutes. **Table 3** compares the percentage conversion of myristic acid for (i) intact $OleT_{JE}$-HRV3C-AldO, (ii) cleaved $OleT_{JE}$-HRV3C-AldO, and (iii) $OleT_{JE}$-αhelix-AldO, as well as the concentrations of tridecene, 2-OH myristic acid and 3-OH myristic acid products formed. For all proteins, there was little activity at 0.01% glycerol. However, hydroxylated products were formed at higher levels than alkene at low glycerol concentrations. At 0.1% glycerol, levels of 2-OH and 3-OH myristic acid are higher than at 1% glycerol. This may occur due to limited enzymatic activity at the lower glycerol concentration, resulting in less efficient secondary oxidation of the primary hydroxylated reaction products.

For intact $OleT_{JE}$-HRV3C-AldO, the 1% glycerol condition yielded a 15% increase in total turnover and 9% increase in alkene production compared to 0.1% glycerol. There was little difference in total turnover and alkene levels for the intact and HRV3C-cleaved forms of $OleT_{JE}$-HRV3C-AldO, suggesting that proteolytic cleavage is effective and does not inactivate enzymatic functions.

Secondary turnover of 2-OH myristic acid and 3-OH myristic acid products

Time-course reactions with $OleT_{JE}$-AldO fusion proteins showed that levels of 2-OH and 3-OH myristic acid decreased over time (from ~2 minutes onwards). This suggested that $OleT_{JE}$ can convert these hydroxylated fatty acids to further products (**Figure 6**). 0.5 ml reactions were set up with 5 µM $OleT_{JE}$-HRV3C-AldO, 1% glycerol and 200 µM of either 2-OH or 3-OH myristic acid, or using 1 µM $OleT_{JE}$/500 µM H_2O_2. Previous studies on the *S. coelicolor* AldO enzyme reported a k_{cat} = 17 s^{-1} and a k_{cat}/K_m = 1.2 x 10^4 M^{-1} s^{-1} for sorbitol, and values of k_{cat} = 13 s^{-1} and k_{cat}/K_m = 4.1 x 10^4 M^{-1} s^{-1} for xylitol at pH 7.5 (26); and a k_{cat}/K_m = 2.1 x 10^4 M^{-1} s^{-1} for glycerol at pH 9.0 (27). Given the similar extents of oxidation of these different substrates by the $OleT_{JE}$-HRV3C-AldO fusion enzyme (**Table 2**), it is likely that the kinetics of this fusion enzyme are similar to those reported previously.

Reactions were incubated for 30 minutes with mixing at 700 rpm at 27°C. GC/Q-TOF chromatograms were compared to those of control samples without enzyme. Data showed that both 2-OH and 3-OH myristic acid were used effectively as $OleT_{JE}$ substrates, with 3-OH myristic acid reactions showing almost complete turnover (**Figure 7**). For the 2-OH myristic acid reaction, two products were identified. One of these products is tridec-1-en-1-ol, indicating that $OleT_{JE}$ can decarboxylate 2-OH myristic acid. The ion spectrum of the second product indicates that it is 2-hydroxytetradec-2-enoic acid. This demonstrates that $OleT_{JE}$ can desaturate 2-OH myristic acid at the C_{α}-C_{β} bond. For reactions with 3-OH myristic acid, the product is 3,4 dihydroxytetradec-2-enoic acid, indicating that $OleT_{JE}$ can further hydroxylate as well as desaturate 3-OH myristic acid.

Discussion

The *Jeotgalicoccus* sp. $OleT_{JE}$ is an efficient P450 peroxygenase that uses H_2O_2 to oxidatively decarboxylate fatty acids to form terminal alkenes. This peroxide shunt mechanism (**Figure 1**) to form compound 0 is inefficient in many P450s, including BM3, causing heme oxidative damage and giving low product formation. Efforts have been made to enhance peroxide shunt efficiency through protein engineering of BM3 and the camphor hydroxylase P450cam, although improvements were not substantial (28,29). Our data (using heme stability analysis) show that $OleT_{JE}$ is relatively tolerant to H_2O_2, and clearly more resistant to H_2O_2-mediated heme oxidation than are the BM3, CYP121A1 and CYP51B1 P450s (**Figure 3**, **Table 1**). Even after incubation of $OleT_{JE}$ with 1 mM H_2O_2, its Fe^{II}-CO spectrum remains almost completely in the P450 (A_{max} = 449 nm) form, indicative of negligible loss of its cysteine thiolate heme ligand. However, despite its evolution into a peroxygenase, it remains somewhat susceptible to heme modification at higher concentrations of H_2O_2 (e.g. 1-2 mM), although the enzyme should not encounter such elevated levels of H_2O_2 in the bacterial cell.

In this study, we report the production and catalytic properties of AldO-$OleT_{JE}$ fusion systems. AldO produces H_2O_2 as a co-product from oxidation of substrates including glycerol, sorbitol and xylitol. The fused $OleT_{JE}$ uses the H_2O_2 to drive decarboxylation and hydroxylation of myristic acid, a good substrate for $OleT_{JE}$ (7). In a system where $OleT_{JE}$ and AldO proteins are fused by a linker containing a HRV3C cleavage site ($OleT_{JE}$-HRV3C-AldO), addition of 1% glycerol gave an 8% increase in myristic acid conversion compared to addition of 0.5 mM H_2O_2 (following a 20 minute incubation). Glycerol is abundant and inexpensive (30), and is formed as a by-product in the production of biofuels, with associated disposal costs (31). Glycerol would thus be an ideal substrate for cheap and efficient alkene production using AldO-$OleT_{JE}$ fusion enzymes.

The kinetics of myristic acid oxidation and product formation were measured for (i) $OleT_{JE}$-HRV3C-AldO, (ii) $OleT_{JE}$-αhelix-AldO, a construct in which $OleT_{JE}$ and AldO are fused by a non-cleavable alpha helical linker, and (iii) the separated $OleT_{JE}$ and AldO entities produced stoichiometrically by HRV3C-dependent cleavage of the $OleT_{JE}$-HRV3C-AldO linker. The fused proteins showed higher rates of myristic acid turnover than their separated entities, with 97% myristic acid turnover catalysed by $OleT_{JE}$-αhelix-AldO after 20 minutes. Fusion of partner domains thus enhances product formation in comparison to equal amounts of isolated $OleT_{JE}$ and AldO. The ability to co-express functional and stable $OleT_{JE}$/AldO fusion enzymes is also advantageous in producing catalytically self-sufficient enzymes. The proximity of these domains in the fusion enzymes may enhance activity through more

efficient channelling of H_2O_2 between the enzyme active sites, and in a cellular context this could be important in ensuring that fatty acid decarboxylation/hydroxylation is well coupled to H_2O_2 production. The regulated and continuous glycerol-dependent production of H_2O_2 from the $OleT_{JE}$/AldO fusion enzymes described here is likely conducive to more efficient fatty acid oxidation. Previous studies of bacterial peroxygenases have also used such continuous H_2O_2 production strategies (e.g. a light-driven H_2O_2-producing system) (13,32). Our ongoing studies involve analysis of product formation from the $OleT_{JE}$-AldO fusion enzymes expressed in *E. coli* cells to establish reaction efficiency and products formed.

Importantly, time-dependent studies of myristic acid product formation from $OleT_{JE}$-AldO fusion enzymes indicated the early formation and then decrease in concentration of 2-OH and 3-OH myristic acid products. Reactions done at lower glycerol concentration (0.1%) produced higher levels of hydroxylated myristic acid, possibly due to decreased levels of secondary turnover of the hydroxylated products through weaker enzyme activity at lower glycerol concentrations. Incubation of 2-OH myristic acid with $OleT_{JE}/H_2O_2$, or with $OleT_{JE}$-HRV3C-AldO and 1% glycerol, led to further turnover of 2-OH myristic acid and formation of 2-hydroxytetradec-2-enoic acid and tridec-1-en-1-ol, indicating that $OleT_{JE}$ can decarboxylate 2-OH myristic acid as well as catalysing desaturation of this substrate. Desaturation reactions are among the wide repertoire of molecular transformations catalysed by P450s. These may occur either due to (i) imperfect positioning of the substrate carbon radical that forms following hydrogen abstraction to form P450 compound II (Fe^{IV}-OH), leading to an electron transfer from the carbon radical to the iron, forming a carbocation. Loss of the proton adjacent to the carbocation then results in double bond formation; or (ii) compound II not recombining with the substrate carbon radical, and instead abstracting a hydrogen atom from a carbon adjacent to the radical to form the double bond (33). Parallel reactions also revealed extensive conversion of 3-OH myristic acid, and formation of 3,4 dihydroxytetradec-2-enoic acid. These data demonstrate that $OleT_{JE}$ can di-hydroxylate the fatty acid, in addition to desaturating the C_α-C_β bond. $OleT_{JE}$ was previously shown to produce 2-alkanones from reactions with palmitic acid and stearic acid (C16:0 and 18:0) (34). However, we provide the first examples for the secondary turnover of primary $OleT_{JE}$ reaction products with myristic acid.

In conclusion, we describe the development of novel alditol oxidase-peroxygenase (AldO-$OleT_{JE}$) fusion enzymes that enable production of alkenes using glycerol and other alditol substrates. Further, we use these fusion systems to characterize previously undescribed decarboxylated, hydroxylated and desaturated products formed from primary reaction products (2- and 3-hydroxy myristic acid). These data provide new insights into the catalytic repertoire of $OleT_{JE}$, as well as providing efficient new fusion enzyme systems for alkene production.

Author Contributions statement

AWM, RTB and DL conceived and supervised the study. AWM, SM, K-LT, RTB and KJM designed experiments. SM, K-LT, KJM and NJR performed experiments. SM, KJM, DL and K-LT analysed data. SM, AWM and KJM wrote the manuscript. All authors made manuscript revisions.

REFERENCES

1. Luthra, A., Denisov, I. G., and Sligar, S. G. (2011) Spectroscopic features of cytochrome P450 reaction intermediates. *Arch Biochem Biophys* **507**, 26-35
2. Sligar, S. G., and Gunsalus, I. C. (1979) Proton coupling in the cytochrome P-450 spin and redox equilibria. *Biochemistry* **18**, 2290-2295
3. Munro, A. W., Girvan, H. M., and McLean, K. J. (2007) Variations on a (t)heme - novel mechanisms, redox partners and catalytic functions. *Nat Prod Rep* **24**, 585-609
4. Denisov, I. G., Makris, T. M., Sligar, S. G., and Schlichting, I. (2005) Structure and chemistry of cytochrome P450. *Chem Rev* **105**, 2253-2277
5. Rittle, J., and Green, M. T. (2010) Cytochrome P450 compound I: capture, characterization, and C-H bond activation kinetics. *Science* **330**, 933-937
6. Rude, M. A., Baron, T. S., Brubaker, S., Alibhai, M., Del Cardayre, S. B., and Schirmer, A. (2011) Terminal olefin (1-alkene) biosynthesis by a novel P450 fatty acid decarboxylase. *Appl Environ Microbiol* **77**, 1718-1727
7. Liu, Y., Wang, C., Yan, J., Zhang, W., Guan, W., Lu, X., and Li, S. (2014) Hydrogen peroxide-independent production of alpha-alkenes by OleTJE P450 fatty acid decarboxylase. *Biotechnol Biofuels* **7**, 28
8. Wang, W., and Lu, X. (2013) Microbial Synthesis of Alka(e)nes. *Front Bioeng Biotechnol* **1**, 10
9. Herman, N. A., and Zhang, W. (2016) Enzymes for fatty acid-based hydrocarbon biosynthesis. *Curr Opin Chem Biol* **35**, 22-28
10. Belcher, J., McLean, K. J., Matthews, S., Woodward, L. S., Fisher, K., Rigby, S. E., Nelson, D. R., Potts, D., Baynham, M. T., Parker, D. A., Leys, D., and Munro, A. W. (2014) Structure and biochemical properties of the alkene producing cytochrome P450 $OleT_{JE}$ (CYP152L1) from the *Jeotgalicoccus* sp. 8456 bacterium. *J Biol Chem* **289**, 6535-6550
11. Grant, J. L., Hsieh, C. H., and Makris, T. M. (2015) Decarboxylation of fatty acids to terminal alkenes by cytochrome P450 compound I. *J Am Chem Soc* **137**, 4940-4943
12. Grant, J. L., Mitchell, M. E., and Makris, T. M. (2016) Catalytic strategy for carbon-carbon bond scission by the cytochrome P450 OleT. *Proc Natl Acad Sci U S A* **113**, 10049-10054
13. Zachos, I., Gassmeyer, S. K., Bauer, D., Sieber, V., Hollmann, F., and Kourist, R. (2015) Photobiocatalytic decarboxylation for olefin synthesis. *Chem Commun (Camb)* **51**, 1918-1921
14. Girhard, M., Schuster, S., Dietrich, M., Durre, P., and Urlacher, V. B. (2007) Cytochrome P450 monooxygenase from *Clostridium acetobutylicum*: a new alpha-fatty acid hydroxylase. *Biochem Biophys Res Commun* **362**, 114-119
15. Seaver, L. C., and Imlay, J. A. (2001) Hydrogen peroxide fluxes and compartmentalization inside growing *Escherichia coli*. *J Bacteriol* **183**, 7182-7189
16. Girhard, M., Kunigk, E., Tihovsky, S., Shumyantseva, V. V., and Urlacher, V. B. (2013) Light-driven biocatalysis with cytochrome P450 peroxygenases. *Biotechnol Appl Biochem* **60**, 111-118
17. Heuts, D. P., van Hellemond, E. W., Janssen, D. B., and Fraaije, M. W. (2007) Discovery, characterization, and kinetic analysis of an alditol oxidase from *Streptomyces coelicolor*. *J Biol Chem* **282**, 20283-20291
18. van Hellemond, E. W., Vermote, L., Koolen, W., Sonke, T., Zandvoort, E., Heuts, D. P. H. M., Janssen, D. B., and Fraaije, M. W. (2009) Exploring the biocatalytic scope of alditol oxidase from *Streptomyces coelicolor*. *Adv Synth Catal* **351**, 1523-1530

19. Kapust, R. B., Tozser, J., Fox, J. D., Anderson, D. E., Cherry, S., Copeland, T. D., and Waugh, D. S. (2001) Tobacco etch virus protease: mechanism of autolysis and rational design of stable mutants with wild-type catalytic proficiency. *Protein Eng* **14**, 993-1000
20. Butler, C. F., Peet, C., Mason, A. E., Voice, M. W., Leys, D., and Munro, A. W. (2013) Key mutations alter the cytochrome P450 BM3 conformational landscape and remove inherent substrate bias. *J Biol Chem* **288**, 25387-25399
21. McLean, K. J., Carroll, P., Lewis, D. G., Dunford, A. J., Seward, H. E., Neeli, R., Cheesman, M. R., Marsollier, L., Douglas, P., Smith, W. E., Rosenkrands, I., Cole, S. T., Leys, D., Parish, T., and Munro, A. W. (2008) Characterization of active site structure in CYP121. A cytochrome P450 essential for viability of *Mycobacterium tuberculosis*. *J Biol Chem* **283**, 33406-33416
22. McLean, K. J., Warman, A. J., Seward, H. E., Marshall, K. R., Girvan, H. M., Cheesman, M. R., Waterman, M. R., and Munro, A. W. (2006) Biophysical characterization of the sterol demethylase P450 from *Mycobacterium tuberculosis*, its cognate ferredoxin, and their interactions. *Biochemistry* **45**, 8427-8443
23. Hsieh, C. H., and Makris, T. M. (2016) Expanding the substrate scope and reactivity of cytochrome P450 OleT. *Biochem. Biophys. Res. Commun*. **476**, 462-466
24. Amet, N., Lee, H.-F., and Shen, W.-C. (2009) Insertion of the designed helical linker led to increased expression of Tf-based fusion proteins. *Pharm Res* **26**, 523-528
25. Chen, X., Zaro, J., and Shen, W.-C. (2013) Fusion protein linkers: Property, design and functionality. *Adv Drug Deliv Rev* **65**, 1357-1369
26. Heuts, D. P. H. M., van Hellemond, E. W., Janssen, D. B., and Fraiije, M. W. (2007) Discovery, characterization, and kinetic analysis of an alditol oxidase from *Streptomyces coelicolor*. *J Biol Chem* **282**, 20283-20281
27. Gerstenbruch, S., Wulf, H., Mussmann, N., O'Connell, T., Maurer, K.-H., and Bornscheuer, U. T. (2012) Asymmetric synthesis of D-glyceric acid by an alditol oxidase and directed evolution for enhanced oxidative activity towards glycerol. *Appl. Microbiol. Biotechnol*. **96**, 1243-1252
28. Joo, H., Lin, Z., and Arnold, F. H. (1999) Laboratory evolution of peroxide-mediated cytochrome P450 hydroxylation. *Nature* **399**, 670-673
29. Li, Q. S., Ogawa, J., and Shimizu, S. (2001) Critical role of the residue size at position 87 in H_2O_2- dependent substrate hydroxylation activity and H2O2 inactivation of cytochrome P450BM-3. *Biochem Biophys Res Commun* **280**, 1258-1261
30. Mattam, A. J., Clomburg, J. M., Gonzalez, R., and Yazdani, S. S. (2013) Fermentation of glycerol and production of valuable chemical and biofuel molecules. *Biotechnol Lett* **35**, 831-842
31. Yazdani, S. S., and Gonzalez, R. (2007) Anaerobic fermentation of glycerol: a path to economic viability for the biofuels industry. *Curr Opin Biotechnol* **18**, 213-219
32. Amaya, J. A., Rutland, C. D., and Makris, T. M. (2016) Mixed regiospecificity compromises alkene synthesis by a cytochrome P450 peroxygenase from *Methylobacterium populi*. *J Inorg Biochem* **158**, 11-16.
33. Ortiz de Montellano, P. R. (2015) Substrate oxidation by cytochrome P450 enzymes. Pp. 111-176 in Cytochrome P450: Structure, Mechanism and Biochemistry, 4th Ed. Ed. Ortiz de Montellano, P.R. Published by Springer Internation Publishing Switzerland.

34. Dennig, A., Kuhn, M., Tassoti, S., Thiessenhusen, A., Gilch, S., Bulter, T., Haas, T., Hall, M., and Faber, K. (2015) Oxidative decarboxylation of short-chain fatty acids to 1-alkenes. *Angew Chem Int Ed Engl* **54**, 8819-8822
35. Groves, J. T. (2006) High-valent iron in chemical and biological oxidations. *J Inorg Biochem* **100**, 434-447
36. Fisher, M. T., and Sligar, S. G. (1985) Control of heme protein redox potential and reduction rate: linear free energy relation between potential and ferric spin state equilibrium. *J Am Chem Soc* **107**, 5018-5019

FIGURES

Figure 1. P450 catalytic cycle and active site structure of $OleT_{JE}$. Panel A shows a cytochrome P450 catalytic cycle, illustrating how $OleT_{JE}$ utilises the peroxide shunt pathway to catalyse fatty acid decarboxylation to form terminal alkenes. In its ferric resting state, the $OleT_{JE}$ heme iron is axially co-ordinated by cysteine thiolate and a water molecule. Upon addition of fatty acid (a), the axial water molecule is displaced, and the heme iron converts from a low spin (LS) to a high spin (HS) state (2). Addition of H_2O_2 to $OleT_{JE}$ initiates the peroxide shunt, forming a ferric-hydroperoxo intermediate (Compound 0, reaction indicated by the arrow crossing the cycle). Protonation and dehydration of Compound 0 (f), yields a reactive ferryl (Fe^{IV})-oxo, porphyrin radical cation (Compound I), which has been observed in $OleT_{JE}$ using single turnover stopped-flow absorption spectroscopy (11). $OleT_{JE}$ then catalyses either decarboxylation of the fatty acid (g-i) to form terminal alkene (the major reaction), or hydroxylates the substrate at the α- or β-position (not shown). Hydroxylation involves Compound I-mediated hydrogen abstraction from a substrate CH group (forming Compound II, Fe^{IV}-OH), and hydroxylation by radical rebound with restoration of the ferric heme (35). However, decarboxylation likely occurs through the further abstraction of an electron from the substrate radical by Compound II (h), producing an unstable substrate carbocation or diradical that decarboxylates to generate the alkene (12). The alkene product then dissociates, releasing CO_2 (i), and a protonation step restores the ferric heme iron to its resting, water ligated form. $OleT_{JE}$ can also function using redox partner systems, in which case two electron transfer steps and one protonation step are required to convert the substrate-bound, ferric species to compound 0 [(b)-(e)] (34,36). Steps (f)-(i) then occur as described above following the peroxide shunt process (3). **Panel B** shows the active site of $OleT_{JE}$ bound to arachidic acid (C20:0), with substrate shown in orange (10) (PDB 4L40). The heme is coloured in blue, and is proximally coordinated to Cys365 thiolate. Also shown is arachidic acid (orange) and the interaction between its carboxylate and Arg245.

Figure 2. Schematic of $OleT_{JE}$-AldO constructs. **Panel A** shows how an $OleT_{JE}$-AldO fusion system can use *S. coelicolor* AldO to oxidise glycerol (or another alditol substrate), forming H_2O_2 as a co-product. H_2O_2 is then used by $OleT_{JE}$ to decarboxylate fatty acids such as myristic acid, producing terminal alkenes as the major product. Terminal alkenes have important potential industrial uses, including as "drop-in" biofuels. **Panel B** shows the fusion constructs used in this work. (i) $OleT_{JE}$-HRV3C-AldO. $OleT_{JE}$ and AldO are fused by a HRV3C-cleavable linker, enabling stoichiometric production of $OleT_{JE}$ and AldO, as shown in (ii). (iii) $OleT_{JE}$-αhelix-AldO. In this construct $OleT_{JE}$ and AldO are linked by an $A(EAAK)_4LEA(EAAK)_4A$ α-helix.

Figure 3. P450 H_2O_2 tolerance. Panels A-D show the UV-visible spectra of $OleT_{JE}$ (**A**), BM3 heme domain (**B**), CYP51B1 (**C**), and CYP121A1 (**D**), before (thick solid line) and after the addition of 1 mM H_2O_2. Proteins are all at a concentration of 5 μM. These spectra show heme absorbance decrease due to H_2O_2-mediated oxidation of the prosthetic group, sampled over 1 hour at 1.5 minute intervals. Rate constants for heme oxidation were obtained for the four proteins at H_2O_2 concentrations between 0.025-2 mM H_2O_2 (see **Table 1**). At 1 mM H_2O_2, the greater stability of $OleT_{JE}$ enzyme compared to the other (non-peroxygenase) P450s is clear, with much greater heme oxidation and absorbance loss observed for BM3 heme domain, CYP51B1 and CYP121A1 compared to $OleT_{JE}$ under the same conditions.

Figure 4: SDS-PAGE analysis of purified $OleT_{JE}$ fusion proteins. **Panel A** shows intact $OleT_{JE}$-HRV3C-AldO (i) and cleaved $OleT_{JE}$-HRV3C-AldO (ii), following incubation of the fusion protein with HRV3C protease for 1 hour at 4°C. **Panel B** shows purified $OleT_{JE}$-αhelix-AldO (iii). Samples were resolved by SDS-PAGE using a 10% polyacrylamide gel. The first lane in each case shows protein markers (NEB Broad Range Protein Ladder).

Figure 5: GC/MS chromatogram showing products formed by the $OleT_{JE}$-αhelix-AldO fusion protein with myristic acid substrate. The reaction shown was performed at 27°C with shaking at 700 rpm, and with 0.5 mM myristic acid, 5 μM $OleT_{JE}$-αhelix-AldO fusion protein and 0.1% glycerol. The black chromatogram shows reaction products formed with the reaction stopped at 20 minutes. The red chromatogram shows a control reaction containing the same components, but also including catalase (40 units) to remove H_2O_2. The peaks relate to the following compounds: i) tridecene, ii) pentadecene (internal standard), iii) myristic acid, iv) 2-OH myristic acid, v) 3-OH myristic acid, and vi) palmitic acid (internal standard).

Figure 6. Time dependence of myristic acid conversion and product formation at 1% glycerol. **Panels A, B and C** show the extents of myristic acid conversion using GC/MS data collected following stopping the reaction immediately after its initiation (~10 s), and then after 0.5, 1, 2, 5, 10 and 20 minutes for intact $OleT_{JE}$-HRV3C-AldO, cleaved $OleT_{JE}$-HRV3C-AldO and $OleT_{JE}$-αhelix-AldO, respectively. **Panels D, E and F** show concentrations of tridecene, 2-OH myristic acid and 3-OH myristic acid in samples taken over 20 minutes for the same enzymes. Duplicate samples were tested and standard errors are shown.

Figure 7. Secondary turnover of primary hydroxylated products from $OleT_{JE}$-HRV3C-AldO fusion protein-mediated myristic acid oxidation. **Panel A** shows chromatograms from a reaction (black) with 5 μM $OleT_{JE}$-HRV3C-AldO fusion protein, 200 μM 2-OH myristic acid and 500 μM H_2O_2, as well as a control sample with no enzyme (red). The reaction shows a decrease in 2-OH myristic acid (ii) and the appearance of peaks (i) and (iii). The ion spectra identify these molecules as (i) tridec-1-en-1-ol and (iii) 2-hydroxytetradec-2-enoic acid. **Panel B** shows reaction (black) and control (red) with 200 μM 3-OH myristic acid (same conditions as for panel A). The data show the disappearance of 3-OH myristic acid (iv), and the appearance of peak (v), which is identified as 3,4 dihydroxytetradec-2-enoic acid.

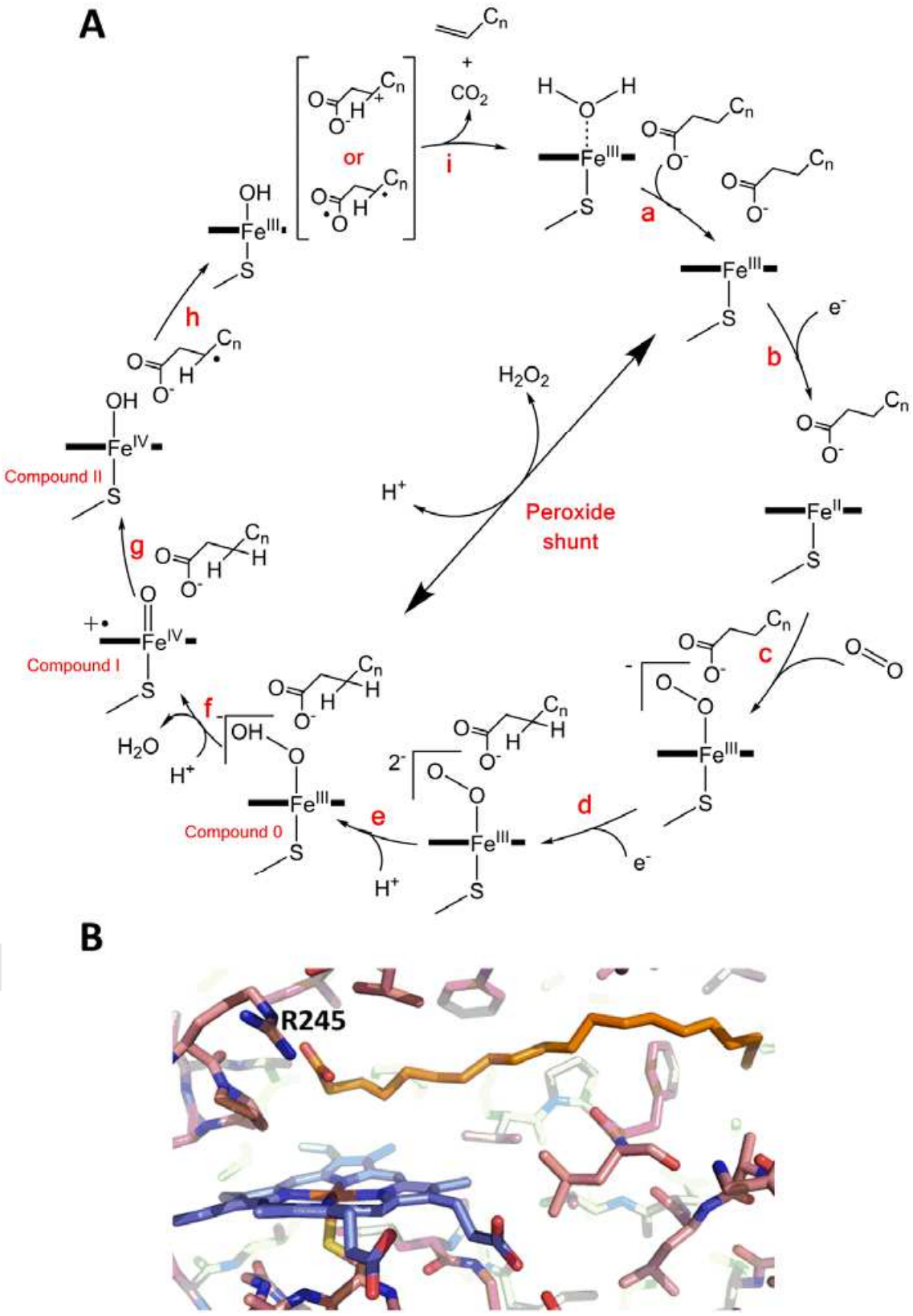

Figure 1

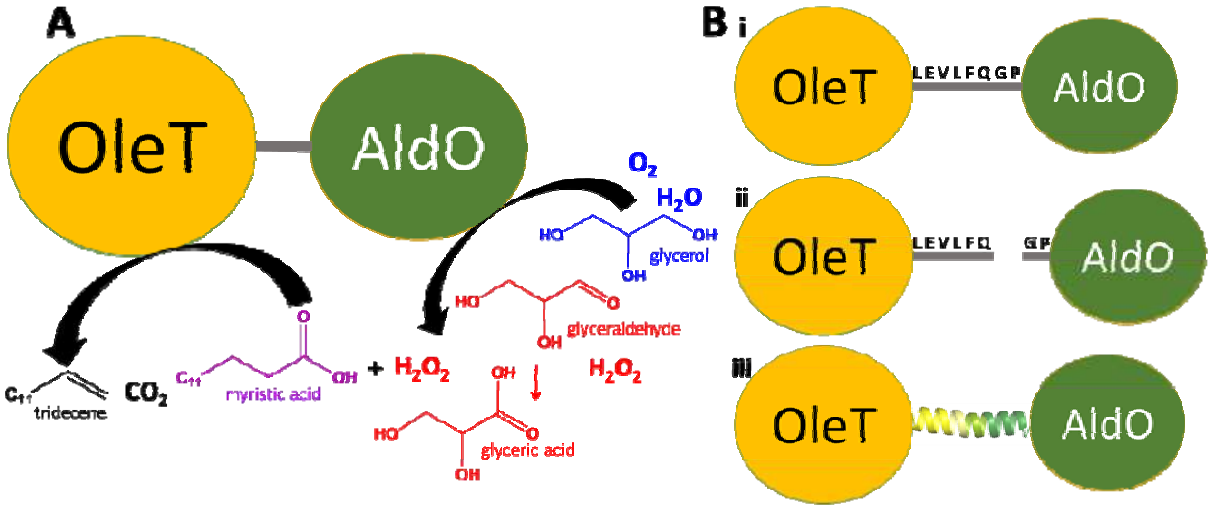

Figure 2

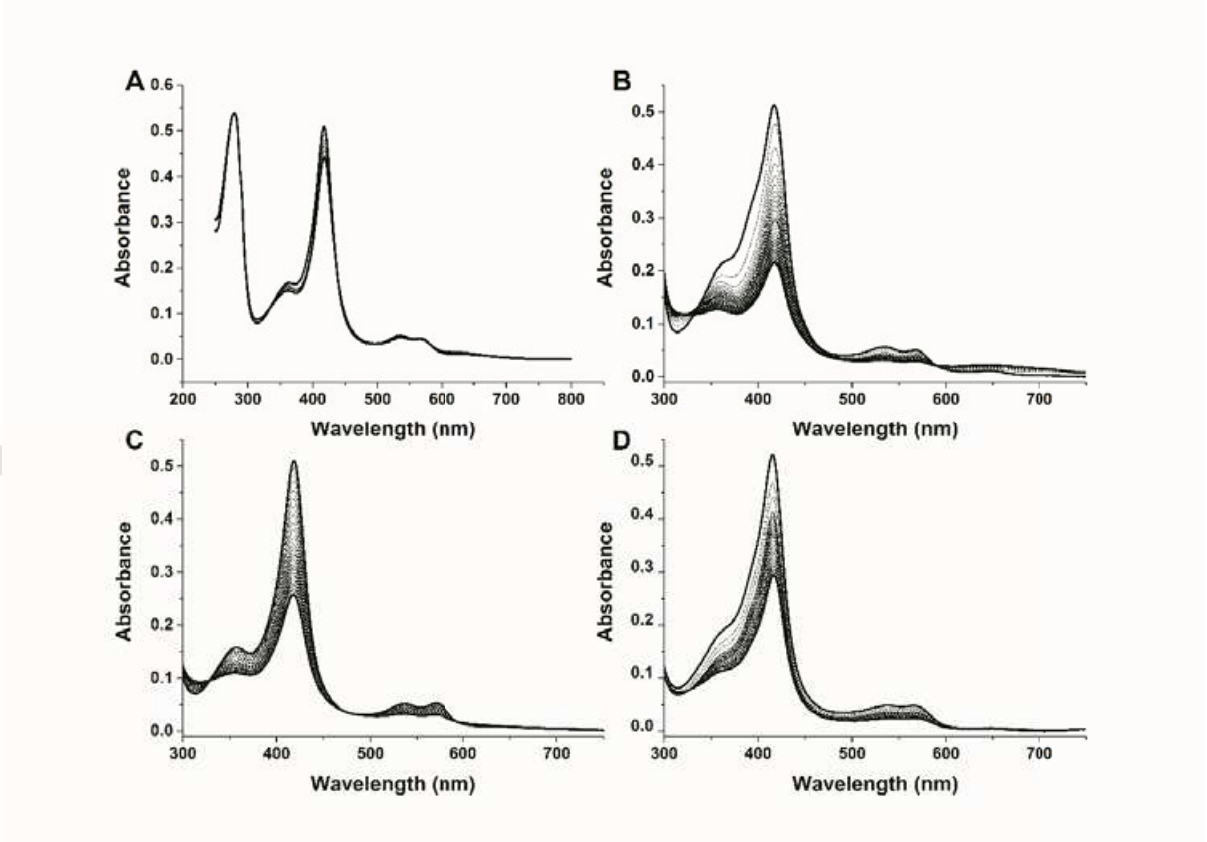

Figure 3

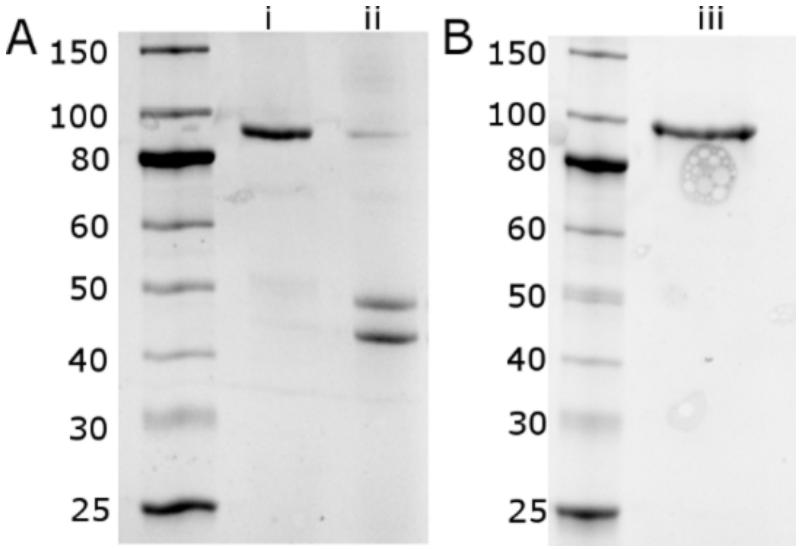

Figure 4

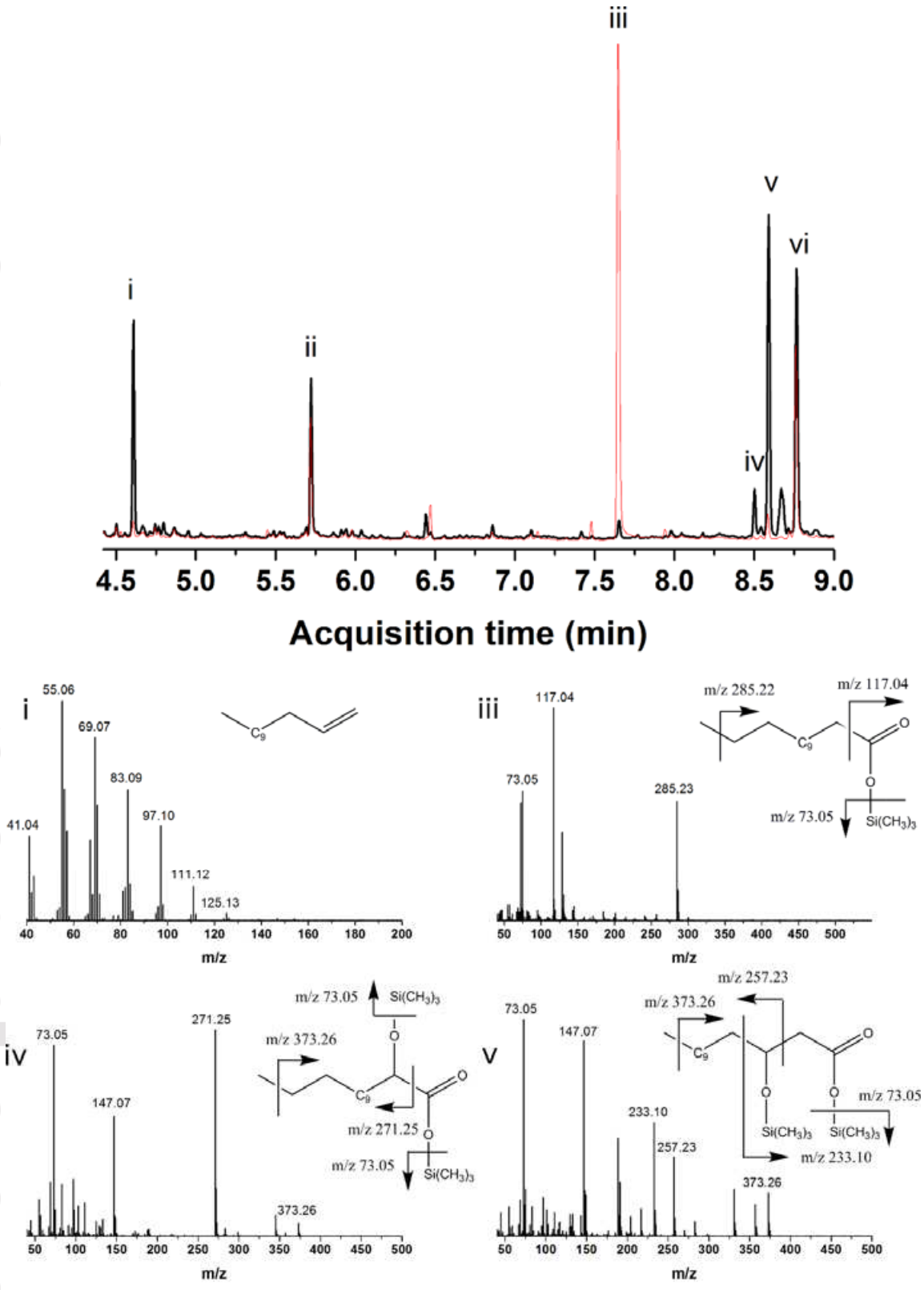

Figure 5

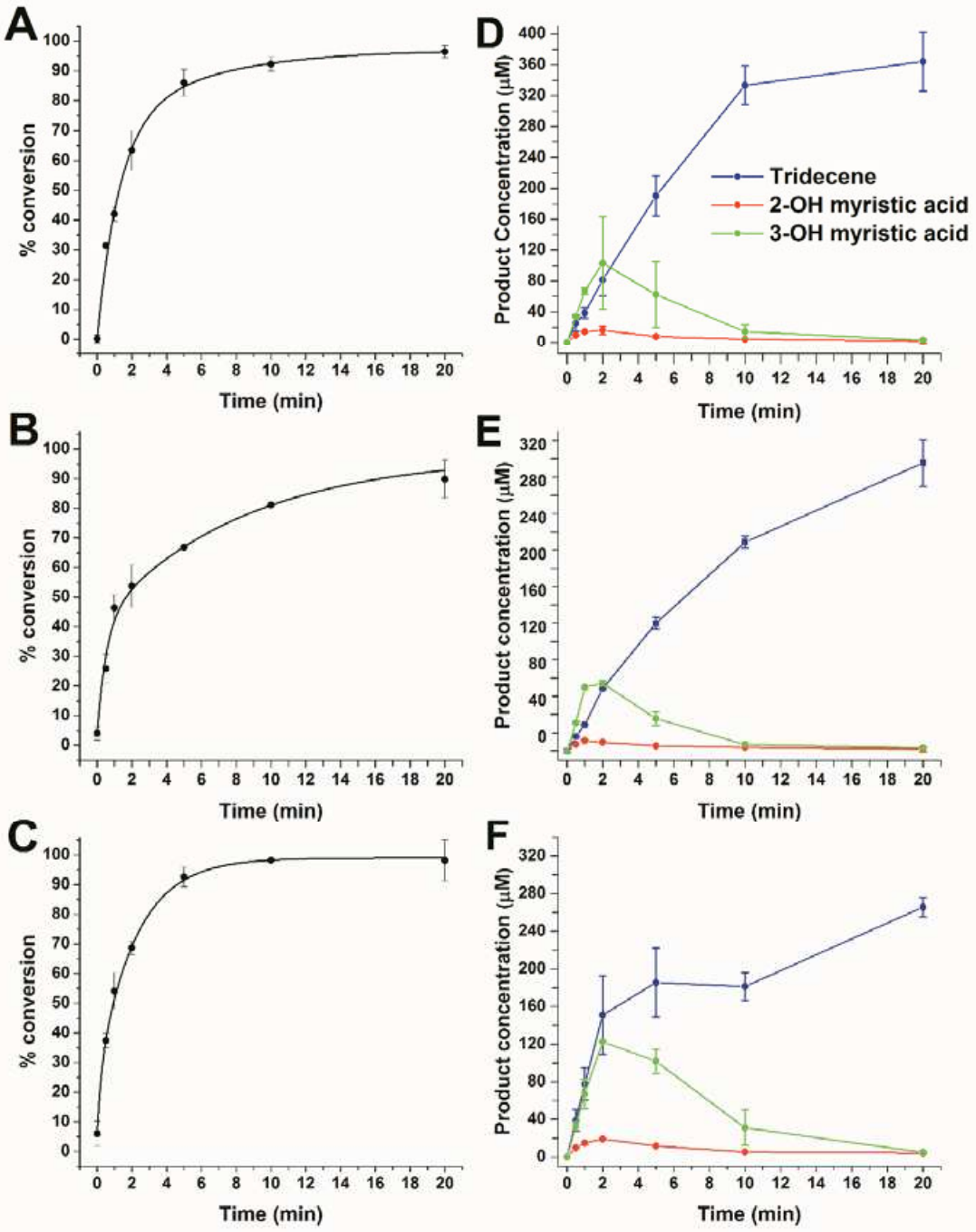

Figure 6

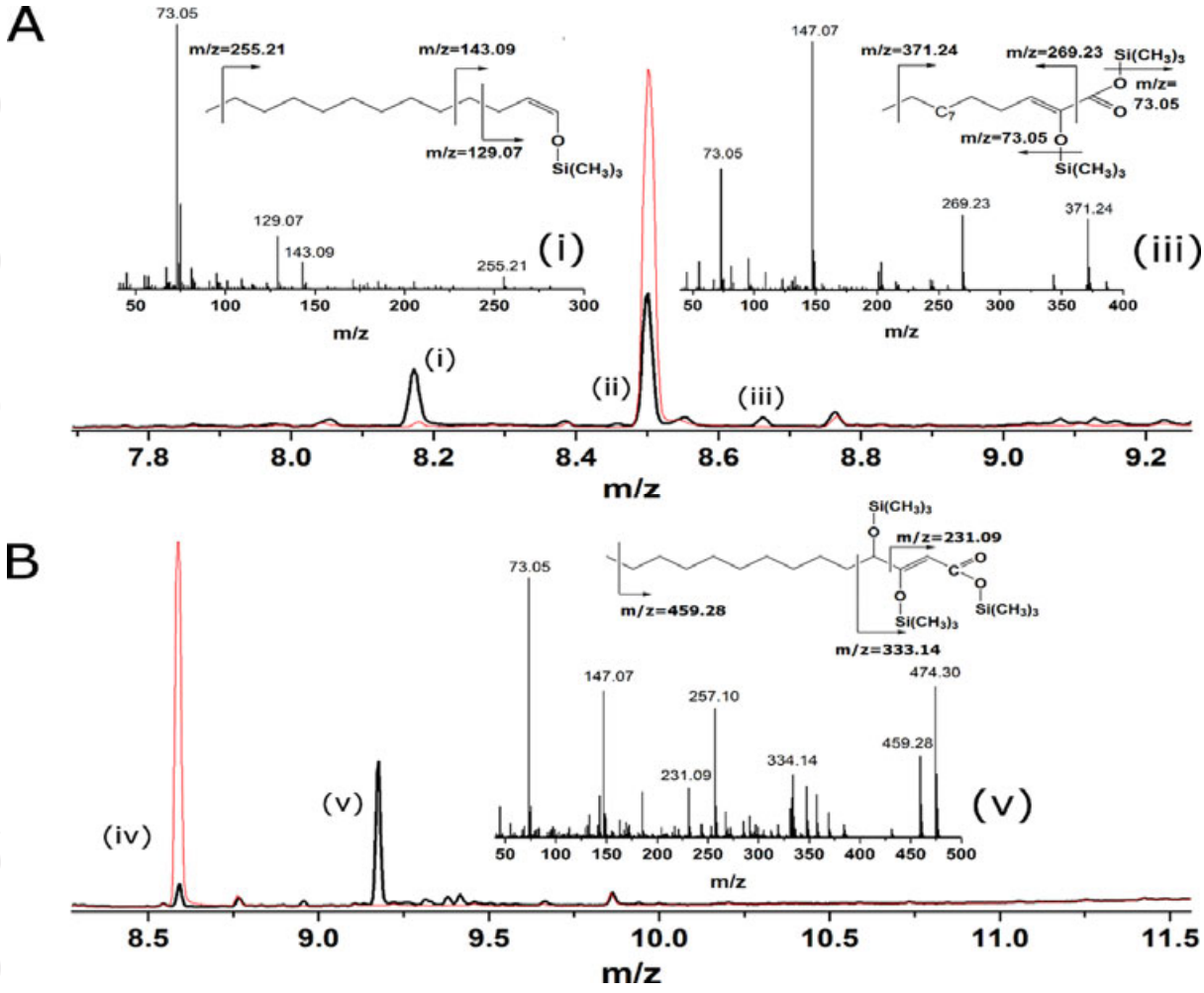

Figure 7

Table 1. Rates of oxidative modification of $OleT_{JE}$, P450 BM3 heme domain, CYP51B1 and CYP121A1 by H_2O_2. Rate constants for heme oxidation (*k*) and associated absorbance amplitudes (A) for heme Soret peak absorption change are presented for $OleT_{JE}$ (418 nm), BM3 heme domain (419 nm), CYP121A1 (417 nm) and CYP51B1 (418 nm) across a range of H_2O_2 concentrations. Data were fitted using a single exponential function. ND indicates that rate constants could not be determined accurately due to small amplitudes of heme absorbance change at the lowest concentrations of H_2O_2 or (in the case of CYP51B1 and H_2O_2 concentrations of 0.125 and 0.075 mM) due to linearity of the progress curve.

H_2O_2 (mM)	$OleT_{JE}$		BM3		CYP51B1		CYP121A1	
	k **(min^{-1})**	**A**	***k*** **(min^{-1})**	**A**	***k*** **(min^{-1})**	**A**	***k*** **(min^{-1})**	**A**
2	8.51 ± 0.17	0.182 ± 0.001	43.25 ± 0.26	0.315 ± 0.002	16.14 ± 0.23	0.269 ± 0.004	26.94 ± 0.23	0.221 ± 0.002
1	6.99 ± 0.16	0.065 ± 0.001	22.15 ± 0.17	0.284 ± 0.002	13.84 ± 0.15	0.236 ± 0.009	16.29 ± 0.18	0.193 ± 0.001
0.5	5.65 ± 0.14	0.043 ± 0.001	17.36 ± 0.11	0.257 ± 0.002	10.07 ± 0.11	0.131 ± 0.007	14.36 ± 0.16	0.203 ± 0.001
0.25	4.96 ± 0.13	0.029 ± 0.001	12.60 ± 0.16	0.199 ± 0.002	6.79 ± 0.21	0.058 ± 0.013	9.38 ± 0.11	0.138 ± 0.001
0.125	5.38 ± 0.14	0.021 ± 0.001	9.08 ± 0.11	0.103 ± 0.001	ND	ND	6.96 ± 0.08	0.077 ± 0.001
0.075	5.94 ± 0.12	0.018 ± 0.001	7.23 ± 0.08	0.062 ± 0.001	ND	ND	5.34 ± 0.08	0.023 ± 0.001
0.05	ND	ND	4.36 ± 0.06	0.040 ± 0.001	ND	ND	2.16 ± 0.05	0.013 ± 0.001
0.25	ND	ND	ND	ND	ND	ND	ND	ND

Table 2. $OleT_{JE}$-dependent oxidation of myristic acid with different substrates. The percentage conversion of 0.5 mM myristic acid by the $OleT_{JE}$-HRV3C-AldO fusion enzyme is shown using H_2O_2 and various AldO substrates at different concentrations. A control reaction using 40 units of catalase, myristic acid and $OleT_{JE}$-HRV3C-AldO confirmed that myristic acid oxidation did not occur in the absence of H_2O_2. Myristic acid product analysis was done using GC/MS.

Substrate	Fatty acid conversion (%)
0.5 mM H_2O_2	87 ± 3
1% glycerol	95 ± 3
3% glycerol	94 ± 4
2 mM sorbitol	93 ± 3
10 mM sorbitol	93 ± 2
2 mM xylitol	91 ± 5
10 mM xylitol	92 ± 3

Table 3. Myristic acid conversion by $OleT_{JE}$ fusion enzymes and products formed. Reactions were performed with 0.5 mM myristic acid using (i) intact $OleT_{JE}$-HRV3C-AldO, (ii) cleaved $OleT_{JE}$-HRV3C-AldO, and (iii) $OleT_{JE}$-αhelix-AldO at 0.1% and 1% glycerol concentrations. Reactions were stopped after 20 minutes.

Enzyme system	Glycerol (%)	Tridecene (μM)	2-OH myristic acid (μM)	3-OH myristic acid (μM)	% substrate conversion
(i) $OleT_{JE}$-HRV3C-AldO	1	183 ± 17	0.98 ± 1.40	1.6 ± 0.1	96 ± 1
	0.1	175 ± 6	21 ± 1	93 ± 3.3	81 ± 5
(ii) $OleT_{JE}$ + AldO	1	137 ± 38	1.0 ± 1.4	1.7 ± 0.1	88 ± 3
	0.1	209 ± 19	22 ± 2	113 ± 7	97 ± 1
(iii) $OleT_{JE}$-αhelix-AldO	1	120 ± 2	2.1 ± 0.2	2.4 ± 0.5	98 ± 3
	0.1	118 ± 3	27 ± 2	123 ± 6	93 ± 2